The Astrophysical Journal, 577:85–97, 2002 September 20
© 2002. The American Astronomical Society. All rights reserved. Printed in U.S.A.

HIGH-FREQUENCY VLBA TOTAL AND POLARIZED INTENSITY IMAGES OF GAMMA-RAY BRIGHT BLAZARS

Alan P. Marscher,[1] Svetlana G. Jorstad,[1,2] John R. Mattox,[3] and Ann E. Wehrle[4]
Received 2001 November 28; accepted 2002 May 24

ABSTRACT

We present Very Long Baseline Array images of 42 γ-ray bright blazars, including 36 with polarization vectors, obtained during the course of a multiepoch monitoring program. Each object was observed at either 43 or 22 GHz, with some objects observed at both frequencies and/or at 15 or 8.4 GHz. The morphologies are varied, with some of the blazars displaying long, thin jets, others short, broad jets, and still others containing cores with only very weak features that are probably knots in faint jets. The polarization of the cores ranges from less than 1% to 8.6%, with electric vector position angles (EVPAs) that are split between nearly parallel and nearly transverse to the jet axis. The polarization of knots in the jets covers a much broader range, from less than 2% to tens of percent. The EVPA of the brightest compact feature in each jet ranges from 0° to 80° from the jet position angle, with roughly half measuring less than 20°. The distribution is consistent with intrinsically oblique magnetic fields whose observed directions are altered by relativistic aberration.

Subject headings: galaxies: jets — quasars: general — radio continuum: galaxies — techniques: high angular resolution

1. INTRODUCTION

The γ-ray sources detected by the EGRET detector on the *Compton Gamma Ray Observatory* (Hartman et al. 1999) and at TeV energies by the Whipple Observatory (Buckley 1999) include nearly 70 BL Lacertae objects and quasars with flat radio spectra (which we will collectively refer to as "blazars"). As part of a collaborative effort to determine what other properties of these objects might be related to bright γ-ray emission, we have undertaken a multiepoch Very Long Baseline Array (VLBA) monitoring program of 42 blazars detected by EGRET and Whipple.

We selected blazars for our program based on reported γ-ray detections, requiring that they have neither declinations too far south nor positions too poorly known (accuracy of about 0.″01 is required) to be observed with the VLBA at high frequencies (22 or 43 GHz). A given source was observed at 43 GHz if the flux density of its most compact features was sufficiently high, as indicated by either pronounced variability in brightness or the morphology revealed by previously published maps or our own 22 GHz images. Other sources were observed at 22 GHz. In some cases, it appears in retrospect that the choice of observing frequency was not optimal. For several objects, 15 or 8.4 GHz images were also obtained. This proved particularly important for 0954+556, which appears *not* to be a blazar, since its structure is not sufficiently compact to be imaged at 22 GHz.

Once polarization observations became routine at the VLBA, both the cross- and parallel-hand fringes were correlated. This did not occur until the 1997 observations, near the end of our program, and for most sources we have only one epoch of polarized intensity images. Exceptions are Mrk 421 and Mrk 501, the results of which are reported elsewhere (Marscher 1999), and 1611+343, which showed no appreciable polarization variability over the 1997 April–August period of monitoring.

The time sequences of total intensity images of the blazars in our program and their analysis were presented in Jorstad et al. (2001b). However, that paper contains no information on polarization. In order to complete the compilation of the data, here we present (1) total-intensity images with polarization vectors for those objects observed in 1997 and (2) the best total-intensity images of each source observed only prior to 1997. We discuss briefly the implications of the results.

2. OBSERVATIONS AND DATA ANALYSIS

The observations were carried out with the VLBA recording system using four (before 1996) or eight 8 MHz wide channels in both right and left circular polarization in "snapshot" mode with 3–6 scans of 5–15 minutes duration each. Not all antennas were available at all epochs owing to equipment failures or very poor weather. Initial correlation was carried out at the National Radio Astronomy Observatory (NRAO) Array Operations Center in Socorro, New Mexico. The subsequent calibration was performed at Boston University with the Astronomical Image Processing System (AIPS) software supplied by NRAO, while imaging was performed at Boston University and St. Petersburg State University using the Caltech software DIFMAP (Shepherd 1997). The final images were displayed using AIPS, DIFMAP, and IDL. Determination of the polarization parameters of features on the images was performed with IDL. The calibration included application of the nominal antenna-based gain curves and system temperatures and correction for sky opacity, followed by iterative imaging and phase-plus-amplitude self-calibration. The final flux

[1] Institute for Astrophysical Research, Boston University, 725 Commonwealth Avenue, Boston, MA 02215-1401.
[2] Astronomical Institute, St. Petersburg State University, Bibliotechnaya 2, Peterhof, St. Petersburg 198904, Russia.
[3] Department of Physics and Astronomy, Francis Marion University, Florence, SC 29501-0547.
[4] Jet Propulsion Laboratory, MS 301-486, 4800 Oak Grove Drive, Pasadena, CA 91109.

density scale was adjusted by a scale factor equal to the mean ratio of single-antenna flux density to total flux density in the images of several objects known to have essentially zero extended structure at 22 and 43 GHz. The total flux densities for the last two steps were obtained by interpolating in time the measurements of the monitoring programs at Metsähovi Radio Research Station, Finland, and the University of Michigan Radio Astronomy Observatory.

The polarized intensity observations took place in 1997, mostly on July 30–31. For this epoch, the right-left phase difference was calibrated in AIPS using a scan of 3C 279, while the instrumental polarization "*D*-terms" were determined via the method of Leppänen, Zensus, & Diamond (1995). For each frequency, the final set of *D*-terms was averages over several sources. The electric vector position angle (EVPA) calibration at 43 GHz was obtained by comparison of the EVPAs of components of 3C 279 and 1611+343 with those of Lister, Marscher, & Gear (1998), respectively. At 22 GHz, the noncore components of 1611+343 were used for this purpose. The EVPA calibration was found to be consistent with an independent method that assumes slow variations of the antenna *D*-terms (Leppänin et al. 1995). We used the combined VLBA (1997 November 10) and VLA (1997 November 21) *D*-term data of Gómez et al. (2002) for this purpose. The resulting EVPAs of several sources (e.g., the extended component about 2 mas from the core in CTA 102) are consistent to within $\sim 5^\circ$ with those obtained less than 1 yr earlier and later by various observers, whose own errors are in the 5°–10° range. The EVPA calibration is, therefore, systematically uncertain by $\lesssim 10^\circ$. The polarization of the remainder of the 1997 observations was calibrated using 1611+343, with similar systematic uncertainties.

The images are presented in Figure 1. The levels of the contours, polarization parameters, and other relevant information are listed in Table 1. The parameters of the total intensity model fits (from Jorstad et al. 2001b) and the polarization properties are listed in Table 2 for each bright feature on the images. The dynamic range of the images is limited by calibration errors rather than by thermal noise; this is a common situation in high-frequency very long baseline interferometric observations.

3. JET MORPHOLOGIES

While all sources can be described as having core-jet morphology, in at least one case (0454−234) only the core is apparent above the noise level, although the dynamic range of the image is not high. In 0446+112, 0827+243, and 1741−038 the core region is somewhat extended (i.e., noticeably larger than the resolving beam) with little or no jet emission apparent, and in several other objects (e.g., 0716+714 and 1739+522) the jet emission is very weak. In contrast, in roughly 25% of the cases the jet remains narrow and its emission strong out to considerable angular distance ($\gtrsim 2$ mas) from the core. Even more frequently (about 40% of the sample), the jet is prominent but shorter ($\lesssim 2$ mas). A number of jets display bends, while others, such as 0234+285, 0804+499, 1652+398 (Mrk 501), and 2251+158 (3C 454.3), are very broad. The jet of 1611+343 (DA 406) is narrow out to the position of an extended component.

The quasar 0954+556 appears to be an anomalous case. Fringes were only marginally detected on the shortest baselines at 22 GHz, so we observed the source at 8.4 GHz, at which frequency the detection was stronger, although nearly all the flux density is in overresolved structure. The image in Figure 1 shows two-sided structure with the only possible identification of a core corresponding to a weak feature near the center. Because of the absence of strong, compact features, we conclude that this source is either not a blazar or a very peculiar member of this class. Rather, we suggest that it is a compact symmetric object (Conway et al. 1992) and consider that the association of this quasar with the EGRET source 2EG J0957+5515 (Mattox et al. 1997) is probably spurious.

4. POLARIZATION

The high frequencies of our observations should minimize the effects of Faraday rotation and opacity, except perhaps in the cores of some of the sources (see Taylor 2000). This, combined with the high resolution, allows us to probe the magnetic field configuration of regions in the jet that are as compact as ~ 0.1 mas.

We have compiled and plotted our data to determine whether there are any correlations between fractional polarization and EVPA of the core and between each of these and the apparent velocity of features in the jet. We express the EVPA in terms of the angle χ_a, by which it is inclined relative to the jet axis. The direction of the axis is determined for the core by the position angle of separation between the core and the nearest knot in the jet. For a knot in the jet, the axis is defined as the direction between it and the nearest component between the knot and the core, as determined from Table 3 of Jorstad et al. (2001b).

Table 2 lists the polarization of each feature with both emission above the noise level on the total intensity images and polarization at roughly the noise level or higher. The core polarizations tend to be low, with the highest fractional polarization $m = 8.6\%$ (2209+236) and the lowest less than 1% (six objects). Application of the partial correlation test of Akritas & Siebert (1996), which includes data representing upper and lower limits, reveals that there is no significant correlation between the fractional polarization of the core and redshift.

Figure 2*a* plots χ_a versus percent polarization of the core for those objects in which the latter is detectable (at $>2\ \sigma$). There is only one weak apparent trend: the dearth of cores with $\chi_a \sim 40^\circ$. There is no correlation apparent between χ_a and percent polarization. These conclusions are independent of the frequency of observation. This negative result contrasts with the study by Lister (2001) of the polarization properties of compact extragalactic radio sources from the Pearson-Readhead survey (PR sample; Pearson & Readhead 1988), which revealed a trend between values of χ_a closer to zero and stronger core polarization. The PR sample contains flat-spectrum radio sources, including a number of blazars, but is not as strongly selected for relativistic beaming as are bright γ-ray blazars (see Jorstad et al. 2001b and Lister & Marscher 1999).

Figure 2*b* plots χ_a versus percent polarization of knots in the jet whose polarization is detectable (at $>2\ \sigma$). Again, no correlation is apparent. The distribution of χ_a values is shown in histogram form in Figure 3, which highlights those features that are the brightest moving components of their respective jets. The distribution displays a peak near $\chi_a = 0$ and a deficit near $\chi_a = 90^\circ$. Among the quasars, there is a broad distribution at intermediate angles, while there are no

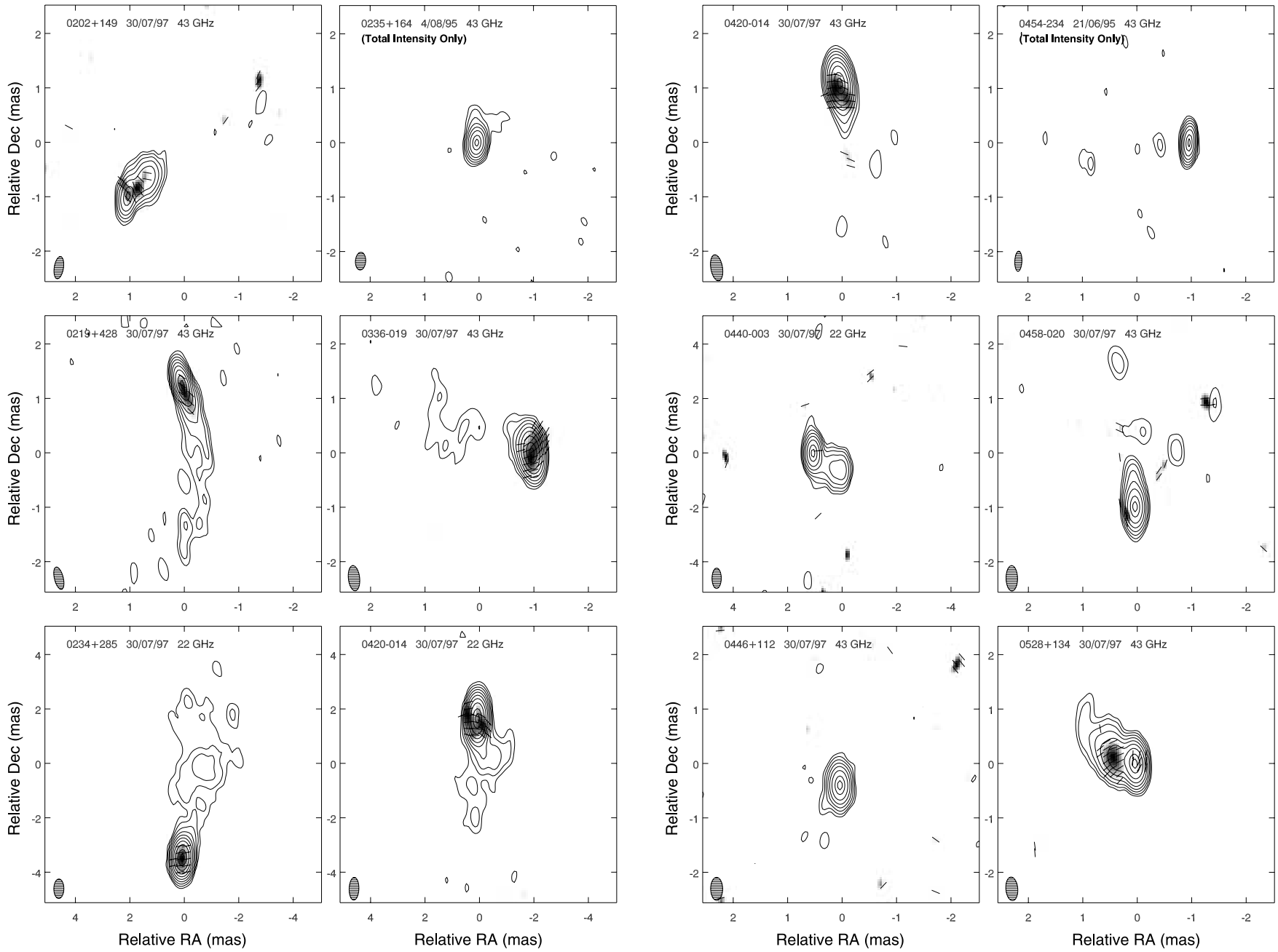

FIG. 1.—Total (*contours*) and polarized (*gray scale*) intensity images of the blazars in our monitoring program. Short straight lines correspond to polarization electric vectors. Only total intensity contours are displayed for sources not observed in 1997. Contour levels and maximum intensities are given in Table 1.

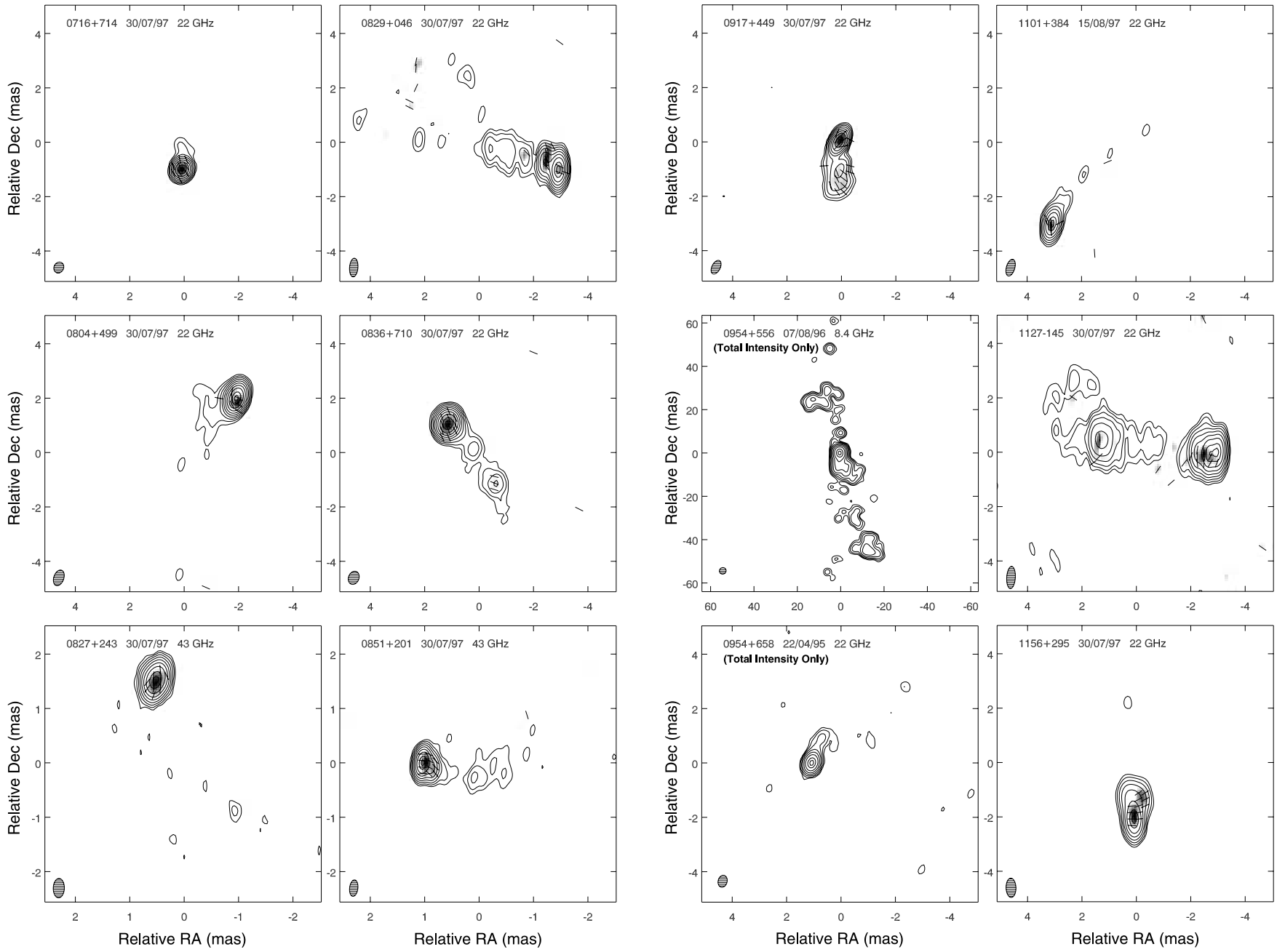

FIG. 1.—*Continued*

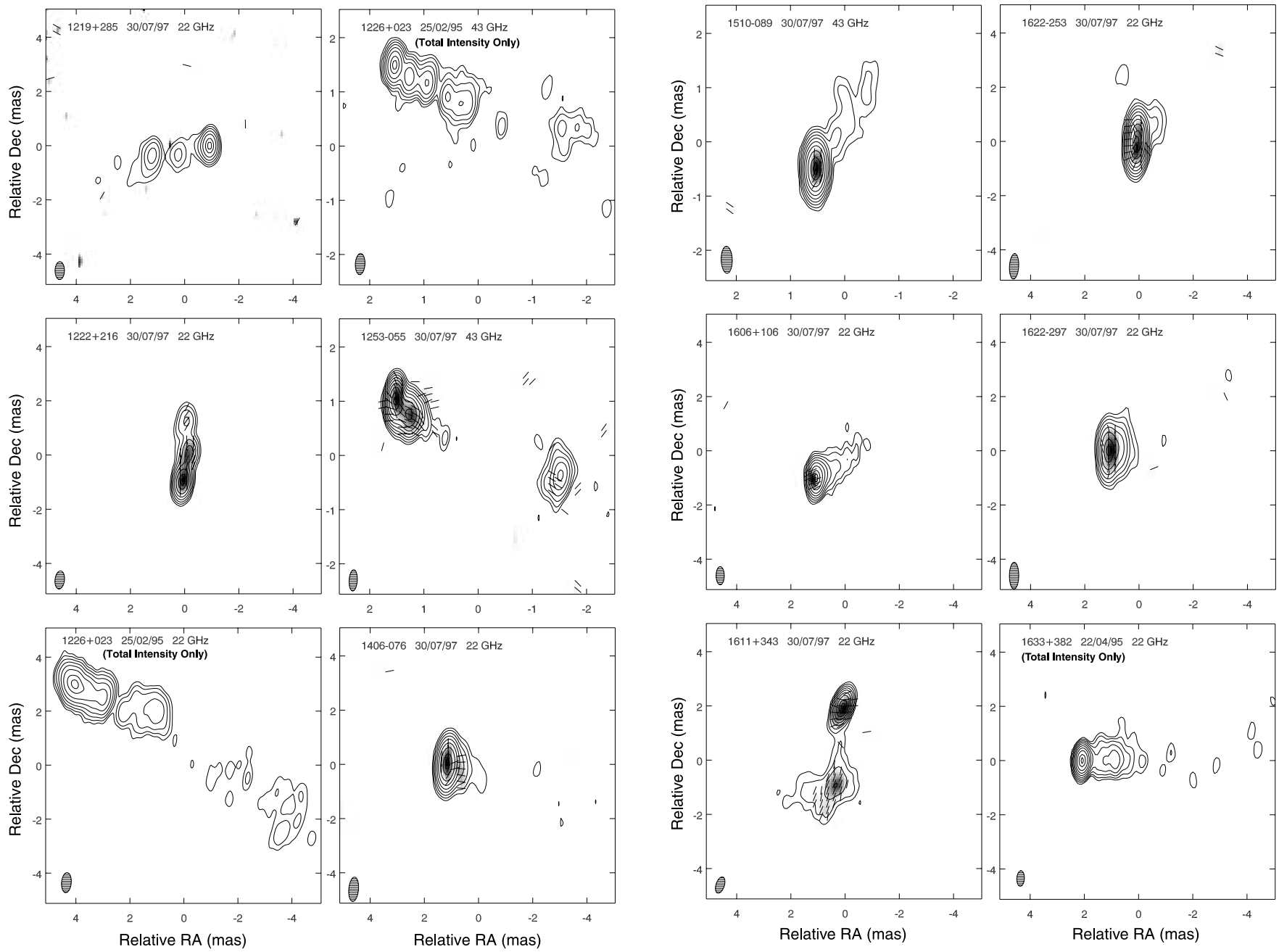

FIG. 1.—*Continued*

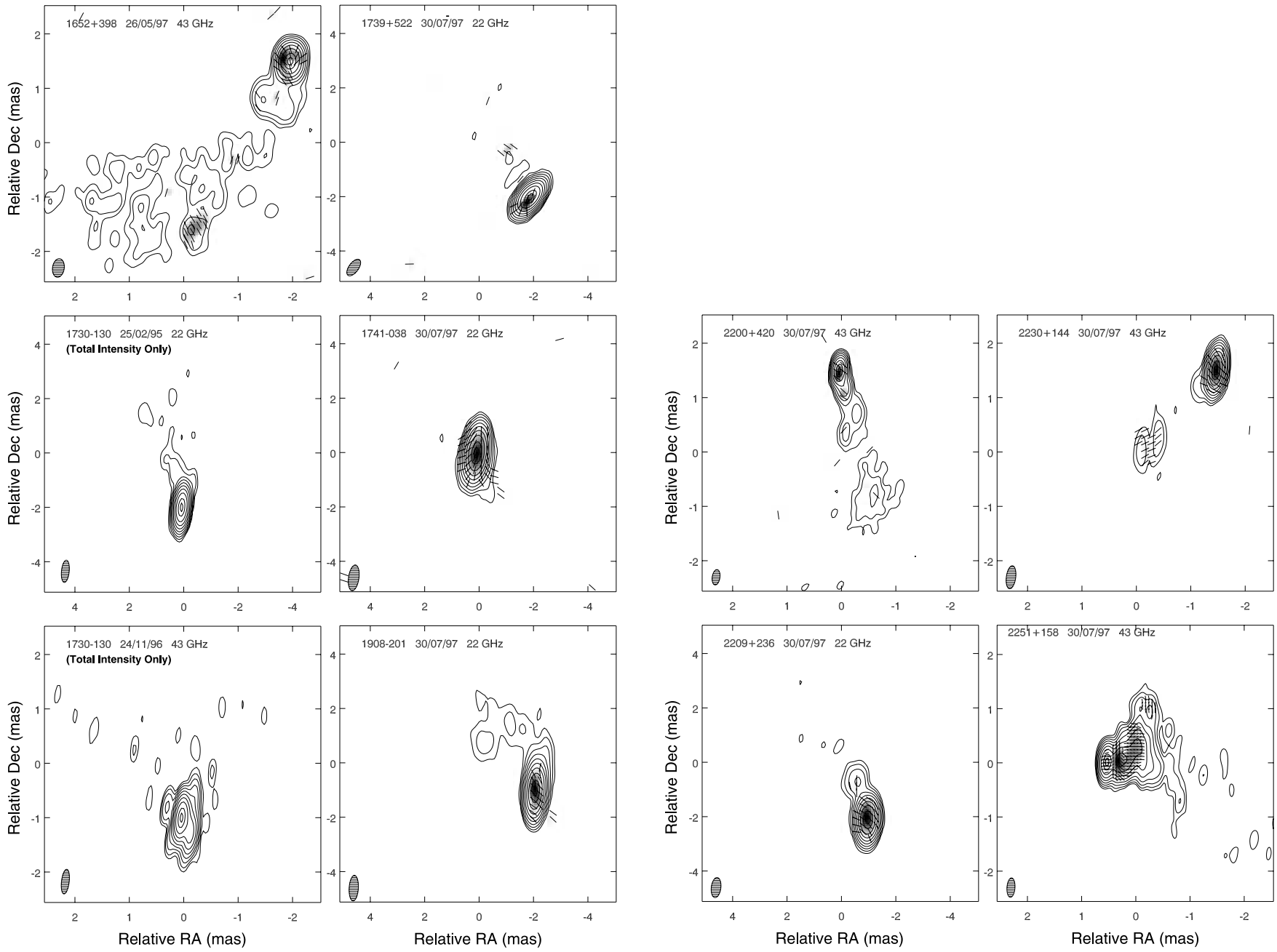

FIG. 1.—*Continued*

TABLE 1

PARAMETERS OF MAPS

Source	Frequency (GHz)	Type[a]	$\Theta_{b,\,\mathrm{maj}}$ (mas)	$\Theta_{b,\,\mathrm{min}}$ (mas)	P.A. (deg)	rms (mJy beam^{-1})	Peak Intensity (mJy beam^{-1})	Contour c_0[b] (%)
0202+149	43.2	I	0.39	0.19	−7	5.8	0.41	2.0
		P	...	...	...	3.4	0.014	...
0219+428 (3C 66A)	43.2	I	0.42	0.16	+14	2.0	0.70	0.5
		P	...	...	...	3.0	0.027	...
0234+285 (CTD 20)	22.2	I	0.62	0.33	−1	2.1	1.45	0.25
		P	...	...	...	2.6	0.069	...
0235+164	43.2	I	0.32	0.19	−4	2.9	0.40	1.0
0336−019 (CTA 26)	43.2	I	0.42	0.19	+7	2.7	1.66	0.5
		P	...	...	...	3.0	0.036	...
0420−014 (OA 129)	22.2	I	0.78	0.34	−1	4.3	3.00	0.25
		P	...	...	...	3.5	0.019	...
	43.2	I	0.42	0.19	+7	7.2	2.56	0.5
		P	...	...	...	3.7	0.033	...
0440−003 (NRAO 190)	22.2	I	0.63	0.36	−1	3.4	0.49	1.0
		P	...	...	...	3.1	0.010	...
0446+112	43.2	I	0.38	0.19	−2	3.7	0.64	1.0
		P	...	...	...	3.3	0.013	...
0454−234	43.2	I	0.37	0.13	−4	2.9	0.46	1.0
0458−020	43.2	I	0.40	0.17	−2	3.9	0.72	1.0
		P	...	...	...	4.4	0.018	...
0528+134	43.2	I	0.37	0.18	+4	4.7	1.71	0.5
		P	...	...	...	3.5	0.049	...
0716+714	22.2	I	0.42	0.34	−24	2.9	1.01	0.5
		P	...	...	...	3.0	0.063	...
0804+499 (OJ 508)	22.2	I	0.54	0.32	−20	1.3	1.10	0.25
		P	...	...	...	1.6	0.011	...
0827+243	43.2	I	0.31	0.18	−6	3.1	1.09	0.5
		P	...	...	...	3.0	0.033	...
0829+046	22.2	I	0.69	0.31	−4	1.8	0.64	0.5
		P	...	...	...	2.6	0.013	...
0836+710	22.2	I	0.45	0.31	−24	1.3	1.79	0.25
		P	...	...	...	1.9	0.056	...
0851+202 (OJ 287)	43.2	I	0.30	0.15	−7	4.7	1.39	0.5
		P	...	...	...	3.9	0.039	...
0917+449	22.2	I	0.53	0.30	−24	2.7	1.01	0.5
		P	...	...	...	1.5	0.016	...
0954+556	8.4	I	3.16	2.96	−68	1.5	0.13	1.0
0954+658	22.2	I	0.45	0.33	−14	1.5	0.56	1.0
1101+384 (Mrk 421)	22.2	I	0.66	0.31	−12	2.6	0.39	1.0
		P	...	...	...	2.0	0.009	...
1127−145	22.2	I	0.81	0.32	−4	2.3	0.83	0.5
		P	...	...	...	2.8	0.014	...
1156+295 (4C 29.45)	22.2	I	0.62	0.31	+3	3.8	0.57	1.0
		P	...	...	...	2.2	0.013	...
1219+285 (ON 231)	22.2	I	0.66	0.34	−1	1.7	0.30	1.0
		P	...	...	...	1.8	0.006	...
1222+216 (4C 21.35)	22.2	I	0.66	0.34	−5	5.2	0.76	1.0
		P	...	...	...	2.2	0.033	...
1226+023 (3C 273)	22.2	I	0.75	0.36	−5	3.4	4.99	1.0
	43.2	I	0.39	0.18	−3	4.4	6.66	0.5
1253−055 (3C 279)	43.2	I	0.39	0.15	−3	11.4	10.9	0.25
		P	...	...	...	23	0.522	...
1406−076	22.2	I	0.78	0.31	−6	3.2	0.86	0.5
		P	...	...	...	1.7	0.017	...
1510−089	43.2	I	0.41	0.17	+1	2.0	2.46	0.25
		P	...	...	...	8.1	0.077	...
1606+106	22.2	I	0.69	0.32	−3	3.8	1.25	0.5
		P	...	...	...	2.2	0.013	...
1611+343 (DA 406)	22.2	I	0.61	0.30	−18	1.9	2.69	0.125
		P	...	...	...	1.9	0.046	...
1622−253	22.2	I	0.82	0.28	−5	2.7	3.20	0.25
		P	...	...	...	3.7	0.042	...
1622−297	22.2	I	0.84	0.28	+1	7.3	1.15	1.0
		P	...	...	...	3.3	0.052	...

TABLE 1—*Continued*

Source	Frequency (GHz)	Type[a]	$\Theta_{b,\,\mathrm{maj}}$ (mas)	$\Theta_{b,\,\mathrm{min}}$ (mas)	P.A. (deg)	rms (mJy beam^{-1})	Peak Intensity (mJy beam^{-1})	Contour c_0[b] (%)
1633+382 (4C 38.41).....	22.2	I	0.57	0.28	−3	1.8	2.21	0.25
1652+398 (Mrk 501).....	43.2	I	0.34	0.21	−8	1.0	0.23	0.5
		P	...	...	...	1.0	0.007	...
1730−130 (NRAO 530).....	22.2	I	0.84	0.28	−6	7.9	9.05	0.25
	43.2	I	0.46	0.14	−7	6.7	7.27	0.5
1739+522.....	22.2	I	0.66	0.30	−38	2.3	1.52	0.25
		P	...	...	...	4.3	0.037	...
1741−038.....	22.2	I	0.83	0.31	−10	2.2	5.71	0.25
		P	...	...	...	4.4	0.197	...
1908−201.....	22.2	I	0.77	0.27	−3	2.2	2.03	0.25
		P	...	...	...	3.0	0.034	...
2200+420 (BL Lac).....	43.2	I	0.30	0.14	−12	2.6	1.71	0.25
		P	...	...	...	3.0	0.044	...
2209+236.....	22.2	I	0.62	0.29	−7	1.0	0.96	0.25
		P	...	...	...	1.4	0.055	...
2230+114 (CTA 102).....	43.2	I	0.36	0.14	−8	1.8	6.11	0.125
		P	...	...	...	4.4	0.186	...
2251+158 (3C 454.3).....	43.2	I	0.36	0.14	−5	2.5	1.13	0.5
		P	...	...	...	3.0	0.091	...

[a] The type I corresponds to the total intensity image; the type P corresponds to the polarized intensity image.

[b] Contour levels are represented by geometric series $c_0(1, \ldots, 2^n)$, where c_0 is the lowest contour level indicated in the table, plus the highest contour level, which is always equal to 90%; e.g., for $c_0 = 0.25$ the contour levels would be 0.25, 0.5, 1, 2, 4, 8, 16, 32, 64, and 90 percent of the peak intensity.

values greater than 45° among the small sample of BL Lac objects. Overall, the distribution is roughly similar to that of the PR sample (see Fig. 39 of Lister 2001) and the less well-selected sample of Lister et al. (1998). It is not as strongly clustered at low values of χ_a as the small sample of mostly BL Lac objects presented by Gabuzda & Cawthorne 2000. As is discussed by Lister et al. (1998) and Lister (2001), the type of distribution observed for the γ-ray blazars is expected for knots whose intrinsic magnetic field direction is oblique to the jet axis, with relativistic aberration causing the observed polarization to tend toward low values of χ_a.

In Figure 4 we plot the percent polarization of knots in the jet versus angular distance from the core, including features for which we obtain only upper limits to the former. With or without the upper limits, no correlation is apparent. We find a similar absence of correlation if projected linear distance is substituted for angular distance (Fig. 5), although there are too few detections of polarization in BL Lac knots to rule out a relationship. Lister (2001), on the other hand, finds a correlation between fractional polarization and projected distance from the core in the PR sample. Given the uncertainties, we cannot make a case for any individual feature being polarized at $\gtrsim 30\%$, with the majority falling below $\sim 15\%$. This is because all knots with detected polarization nominally exceeding 20% have low flux densities compared with the core (ratio $\lesssim 0.15$).

We find no correlation between the fastest well-determined apparent velocity of knots in the jet and either percent polarization (Fig. 6*a*) or χ_a (Fig. 6*b*) of the core. Nor is there a correlation between (1) χ_a and flux density (relative to the core) of knots in the jet, (2) χ_a (core) and flux density (relative to the core) of the brightest knot in the jet, or (3) percent polarization of the core and flux density (relative to the core) of the brightest knot in the jet. (These correlation plots are not shown.)

5. DISCUSSION AND CONCLUSIONS

The heterogeneous images of Figure 1, combined with the absence of any consistent polarization signature, demonstrate that γ-ray bright blazars are not particularly similar in radio morphology beyond their shared core-jet structure. On the other hand, the high apparent superluminal velocities found by Jorstad et al. (2001b) and the high γ-ray fluxes indicate that the sample represents objects with extremely relativistically beamed jets. This further implies that the jet axis points almost directly toward us (Lister & Marscher 1999), at least near the core where the γ-rays most likely originate (see Jorstad et al. 2001a). On the other hand, the high apparent superluminal speeds suggest that, downstream of the core, the angle between the jet axis and the line of sight is not much less than Γ^{-1}, where Γ is the Lorentz factor of the pattern of emission that corresponds to a bright feature in the jet. Jorstad et al. (2001b) reconcile this by pointing out that most of the jets are bent and that bending out of the line of sight of an initially aligned jet is much more likely than bending directly into the line of sight of an initially misaligned jet. We therefore expect our sample to be dominated by jets that are pointing essentially directly at us near the core and bending slightly away from the line of sight downstream.

The most popular explanations for high levels of polarization in a jet are (1) amplification of the longitudinal magnetic field by shearing of the internal jet flow or between the jet and external medium, (2) toroidal buildup of the magnetic field by the process that drives the jet flow away from a black hole/accretion disk system (Meier, Koide, & Uchida 2001), and (3) amplification by a shock wave of that component of an ambient random magnetic field that lies parallel to the shock front (Laing 1980). The ordered component of the magnetic field should be (1) parallel to the jet axis, (2)

TABLE 2

VLBI Component Properties

Source	Frequency (GHz)	Component[a]	Gaussian Model Parameters				Values at Central Peak			
			Flux (Jy)	r (mas)	θ[b] (deg)	a[c] (mas)	I_p (Jy beam^{-1})	δr[d] (mas)	EVPA[d] (deg)	m[d,e] (%)
0202+149.....	43.2	A	0.44	0.00	−43	0.07	0.011	0.04	40 ± 9	2.6 ± 0.8
		B3	0.09	0.26	−43	0.10	0.014	0.03	23 ± 9	15.3 ± 4.8
		B+C	0.40	0.50	−46	0.13	0.009	0.04	79 ± 10	2.7 ± 0.9
0219+428.....	43.2	A	0.63	0.00	−152	0.02	0.024	0.00	55 ± 4	3.8 ± 0.5
		B6	0.19	0.20	−152	0.09	0.027	0.07	53 ± 3	14.6 ± 1.7
		B5	0.09	0.57	−160	0.23				<12
		B4	0.07	1.03	−161	0.38				<26
		B3	0.05	1.80	−170	0.49				<54
		B1	0.05	2.70	−176	0.41				<42
0234+285.....	22.2	A	1.33	0.00	−22	0.06	0.069	0.08	102 ± 1	5.5 ± 0.2
		C1	0.25	0.25	−22	0.12				<2.2
		C2	0.04	1.11	−19	0.28				<18
		C3	0.21	3.20	−11	0.90				<12
0336−019.....	43.2	A	1.75	0.00	+45	0.08	0.036	0.08	112 ± 3	2.3 ± 0.2
		P[f]	0.26	0.23	−45	0.00	0.024	0.00	143 ± 4	9.2 ± 1.3
		C5	0.19	0.19	+37	0.23				<5.3
		C3	0.15	1.45	+70	0.98				<52
0420−014.....	22.2	A	3.00	0.00	−160	0.00	0.014	0.00	64 ± 6	0.5 ± 0.1
		P[f]	0.42	0.33	+76	0.00	0.019	0.00	99 ± 6	4.4 ± 0.9
		B2	0.63	0.47	−161	0.00	0.018	0.08	60 ± 6	2.9 ± 0.6
	43.2	A	1.33	0.00	−166	0.00	0.026	0.00	72 ± 4	2.0 ± 0.3
		P[f]	0.72	0.11	+94	0.00	0.033	0.00	91 ± 4	4.6 ± 0.6
		C1+B2	0.07	0.46	−166	0.20	0.019	0.03	87 ± 9	26 ± 8
		C2	0.05	1.64	−160	0.22				<23
0440−003.....	22.2	A	0.49	0.00	−123	0.10	0.003	0.00	...	<0.6
		B	0.19	1.18	−120	0.44				<6.0
		C	0.07	1.27	−121	0.55				<21
0446+112.....	43.2	A	0.54	0.00	+140	0.05				<1.4
0458−020.....	43.2	A	0.72	0.00	+4	0.07	0.004	0.00	...	<0.6
		B2	0.09	0.51	+4	0.04				<10
		C2	0.03	1.47	+1	0.28				<63
		C1	0.03	1.31	−36	0.01				<29
0528+134.....	43.2	A	1.72	0.00	+71	0.04	0.012	0.00	156 ± 8	0.7 ± 0.2
		B4	0.63	0.32	+71	0.23	0.049	0.04	115 ± 2	10.4 ± 0.6
		B3	0.25	0.54	+57	0.20				<4.4
		D3	0.18	0.97	+37	0.13				<4.9
		D4	0.07	1.60	+58	0.16				<14
0716+714.....	22.2	A	1.05	0.00	+25	0.07	0.063	0.00	27 ± 1	6.2 ± 0.3
		B5	0.04	0.23	+25	0.01				<15
		B4	0.03	0.76	−2	0.43				<46
0804+499.....	22.2	A	1.10	0.00	+43	0.06	0.011	0.17	58 ± 4	1.6 ± 0.2
		C1	0.03	0.27	+43	0.18	0.006	0.02	16 ± 8	22 ± 6
0827+243.....	43.2	A	1.16	0.00	+112	0.04	0.033	0.04	176 ± 3	3.0 ± 0.3
		C	0.11	0.26	+112	0.05	0.008	0.06	124 ± 13	6.8 ± 2.9
0829+046.....	22.2	A	0.61	0.00	+65	0.06	0.009	0.00	60 ± 8	1.5 ± 0.4
		C1	0.09	0.14	+68	0.08				<6.0
		C2	0.13	0.55	+61	0.20	0.013	0.10	25 ± 5	12.7 ± 2.1
		B4	0.03	1.34	+71	0.45	0.010	0.02	42 ± 8	41 ± 11
		B3	0.04	2.10	+66	0.27				<17
		B2	0.06	2.60	+74	0.37				<14
0836+710.....	22.2	A	2.02	0.00	−137	0.13	0.056	0.00	23 ± 1	3.0 ± 0.1
		C1	0.08	0.34	−137	0.24				<6.7
		B	0.06	1.26	−132	0.26				<5.4
		C3	0.06	2.7	−143	0.46	0.009	0.00	69 ± 4	22.7 ± 3.5
0851+202.....	43.2	A	1.45	0.00	−119	0.05	0.039	0.04	83 ± 3	3.2 ± 0.3
		C1	0.23	0.19	−119	0.05	0.023	0.00	42 ± 5	10.6 ± 1.9
		B3	0.05	0.40	−114	0.27				<41
		B2	0.06	1.03	−106	0.18				<22
		C2	0.09	1.38	−93	0.49				<55
0917+449.....	22.2	A	1.04	0.00	+161	0.07	0.016	0.11	129 ± 3	1.9 ± 0.2
		C1	0.06	0.83	+162	0.35				<8.8
		B	0.12	0.99	−177	0.17	0.007	0.13	46 ± 3	13.0 ± 1.4

TABLE 2—*Continued*

Source	Frequency (GHz)	Component[a]	Gaussian Model Parameters				Values at Central Peak			
			Flux (Jy)	r (mas)	θ[b] (deg)	a[c] (mas)	I_p (Jy beam^{-1})	δr[d] (mas)	EVPA[d] (deg)	m[d,e] (%)
		C2	0.12	1.53	+174	0.40				<5.0
1101+384.....	22.2	A	0.39	0.00	−25	0.00	0.009	0.00	4 ± 7	2.2 ± 0.5
		B2	0.03	0.59	−30	0.13				<14
		B1	0.02	1.39	−42	0.66				<63
1127−145.....	22.2	A	1.18	0.00	+92	0.14	0.006	0.08	128 ± 8	0.7 ± 0.2
		B3	0.51	0.37	+92	0.21	0.014	0.12	13 ± 4	3.7 ± 0.5
		B2	0.13	0.80	+96	0.31				<6.0
		C2	0.51	4.21	+83	0.71	0.011	0.20	14 ± 2	7.8 ± 0.6
1156+295.....	22.2	A	0.57	0.00	+9	0.05	0.013	0.08	92 ± 5	2.3 ± 0.4
		B2	0.07	0.79	−21	0.24	0.011	0.06	120 ± 8	15 ± 4
		C+B3	0.21	0.71	+9	0.37				<3.6
		D1	0.03	4.1	+2	1.5				<100
1219+285.....	22.2	A	0.30	0.00	+97	0.07	0.001	0.00	...	<0.4
		B9	0.03	0.45	+97	0.13				<13
		B8	0.04	1.19	+106	0.31				<13
		B7	0.09	2.15	+100	0.28				<5.4
		B6	0.02	2.71	+111	0.56				<43
		B5	0.01	3.50	+92	0.33				<53
		B4	0.02	4.42	+107	0.38				<30
1222+216.....	22.2	A	0.76	0.00	−7	0.06	0.033	0.11	2 ± 2	5.0 ± 0.3
		B3	0.09	0.45	−7	0.16				<5.4
		B2	0.21	1.13	−13	0.23	0.025	0.08	161 ± 3	14.3 ± 1.3
		B1	0.11	2.23	−4	0.35	0.008	0.00	145 ± 6	11.3 ± 2.3
1253−055.....	43.2	A	12.7	0.00	−134	0.09	0.522	0.06	15 ± 1	6.0 ± 0.2
		B3	7.6	0.35	−134	0.21	0.442	0.05	65 ± 1	11.4 ± 0.3
		D	1.7	3.35	−114	0.19	0.103	0.13	62 ± 6	6.5 ± 1.4
1406−076.....	22.2	A	0.90	0.00	−103	0.08	0.017	0.07	173 ± 3	2.0 ± 0.2
		B4	0.08	0.68	−103	0.15	0.008	0.00	79 ± 3	25 ± 3
1510−089.....	43.2	A	2.51	0.00	−34	0.06	0.077	0.00	165 ± 3	3.1 ± 0.3
		B2	0.28	0.22	−20	0.04				<6.0
1606+106.....	22.2	A	1.22	0.00	−54	0.08	0.013	0.16	113 ± 4	1.6 ± 0.2
		C1	0.32	0.29	−54	0.38				<2.3
1611+343.....	22.2	A	2.82	0.00	+158	0.10	0.046	0.11	96 ± 1	2.3 ± 0.1
		C1	0.13	0.46	+158	0.19	0.030	0.03	97 ± 2	22.9 ± 1.8
		B4	0.09	1.33	+174	0.28	0.007	0.03	48 ± 8	7.8 ± 2.3
		C2	0.42	2.90	+176	0.65	0.035	0.00	159 ± 1	31 ± 1
		B2	0.14	3.44	+160	0.42	0.012	0.10	160 ± 2	35 ± 2
		B1	0.09	3.86	+147	0.96				<25
1622−253.....	22.2	A	3.34	0.00	−49	0.08	0.042	0.32	147 ± 2	1.7 ± 0.1
		P[f]	0.33	0.36	+91	0.00	0.021	0.00	96 ± 6	6.2 ± 1.2
		B	0.05	0.85	−49	0.06				<15
1622−297.....	22.2	A	1.26	0.00	−72	0.11	0.052	0.08	177 ± 2	4.6 ± 0.3
		D2	0.56	0.32	−72	0.37				<1.9
1652+398.....	43.2	A	0.23	0.00	+154	0.00	0.007	0.14	48 ± 3	5.7 ± 0.5
		B2	0.039	0.68	+159	0.00	0.003	0.00	159 ± 3	33 ± 3
		B1	0.005	3.5	+150	0.00	0.005	0.00	29 ± 18	87 ± 40
1739+522.....	22.2	A	0.98	0.00	+109	0.07	0.026	0.02	161 ± 4	3.8 ± 0.5
		B2	0.91	0.16	+109	0.24	0.037	0.13	163 ± 3	5.4 ± 0.5
		D3	0.02	1.04	+32	0.34				<68
1741−038.....	22.2	A	6.26	0.00	+111	0.14	0.197	0.08	164 ± 1	3.3 ± 0.1
		B2[f]	0.38	0.30	+111	0.05	0.033	0.02	116 ± 4	9.2 ± 1.2
		B1	0.02	1.60	−158	0.48	0.003	0.14		<12
1908−201.....	22.2	A	2.13	0.00	−10	0.07	0.034	0.08	40 ± 3	1.7 ± 0.2
		B3	0.53	0.31	−18	0.18	0.007	0.10	171 ± 8	2.2 ± 0.6
		B2	0.06	2.06	+4	0.64				<30
		D4	0.05	2.6	+47	0.58				<31
		D5	0.06	2.9	+24	0.65				<30
2200+420.....	43.2	A	1.71	0.00	−169	0.00	0.044	0.04	52 ± 2	2.8 ± 0.2
		B2	0.20	0.41	−169	0.00	0.021	0.00	55 ± 4	10.6 ± 1.6
		B1	0.04	2.50	−163	0.00	0.009	0.00	47 ± 15	21 ± 9
2209+236.....	22.2	A	0.68	0.00	+33	0.04	0.055	0.18	54 ± 1	8.6 ± 0.2
		B3	0.48	0.21	+33	0.11	0.031	0.03	60 ± 1	8.3 ± 0.3
		C	0.05	1.49	+17	0.56	0.007	0.00	178 ± 3	32.8 ± 3.1

TABLE 2—*Continued*

Source	Frequency (GHz)	Component[a]	Gaussian Model Parameters: Flux (Jy)	r (mas)	θ[b] (deg)	a[c] (mas)	Values at Central Peak: I_p (Jy beam^{-1})	δr[d] (mas)	EVPA[d] (deg)	m[d,e] (%)
2230+114.....	43.2	A	6.53	0.00	+135	0.05	0.186	0.00	41 ± 1	3.0 ± 0.1
		C	0.21	1.84	+139	0.55	0.026	0.15	128 ± 2	26.9 ± 2.2
2251+158.....	43.2	A	1.13	0.00	−80	0.03	0.023	0.00	103 ± 4	2.0 ± 0.3
		B3	1.66	0.27	−80	0.20	0.091	0.09	0 ± 1	10.6 ± 0.2
		C	1.25	0.60	−56	0.34	0.045	0.02	89 ± 1	9.5 ± 0.3
		D1	0.28	0.84	−95	0.36				<7.7
		D2[f]	0.35	1.15	−39	0.13	0.012	0.14	3 ± 1	27 ± 1

[a] Designations of components correspond to those in Jorstad et al. 2001b, who list the uncertainties in the Gaussian model parameters. Polarized components (usually upstream of the core) that are not evident in the total intensity images or models are designated as "P."

[b] For the core A, θ gives the position angle of the jet close to the core.

[c] Quantity a is the circular Gaussian FWHM diameter of the component.

[d] Parameter δr is the separation between the component's total intensity and polarized intensity maxima; the values of EVPA and m are given for the position of the peak in polarized intensity I_p of the component; the uncertainties in polarization and EVPA are corrected for non-Gaussian behavior (Wardle & Kronberg 1974); the listed error in EVPA is purely statistical: there is an additional systematic uncertainty in the EVPA calibration of $\lesssim 10°$.

[e] Polarized fraction $m = 100[(Q^2 + U^2)^{1/2}/I]\%$, where I, Q, and U are the Stokes parameters; upper limits correspond to $(\delta I_p/\mathrm{flux})[1 + a^2(\Theta_{b,\max}\Theta_{b,\min})^{-1}]$.

[f] Feature is not included as a "jet component" in the analysis because its location is either outside the apparent boundary of the jet or upstream of the core.

transverse to the jet axis, and (3) parallel to the shock front, i.e., perpendicular to the jet axis for a transverse shock and oblique for an oblique shock. The observed EVPA is perpendicular to the aberrated direction of the magnetic field if the emission is optically and Faraday thin. If at any point the jet bends sufficiently toward the observer that the line of sight falls inside the jet cone, then case 2 becomes a circumferential field (radial electric vectors) surrounding the core. Case 1—and case 3 if the shock is transverse to the jet axis—revert to random polarization.

The distribution of values of χ_a of the cores (Fig. 2*a*) suggests that the magnetic field in the core region might be randomly oriented relative to the jet axis. Inspection of the images of Figure 1, however, leads one to allow that misalignments from directions nearly parallel or perpendicular to the jet could be due to bending of the jet. In addition, the polarization near the core is complex in some sources, so there may be multiple components, including one that is close to parallel or perpendicular to the axis. That is, one cannot use these data to falsify the hypothesis that the dominant magnetic field direction in the core of each blazar is roughly either parallel or transverse to the direction of the jet immediately downstream of the core.

There are several objects in which the polarization vectors suggest the presence of a highly polarized halo, with circumferential magnetic field geometry, surrounding the core:

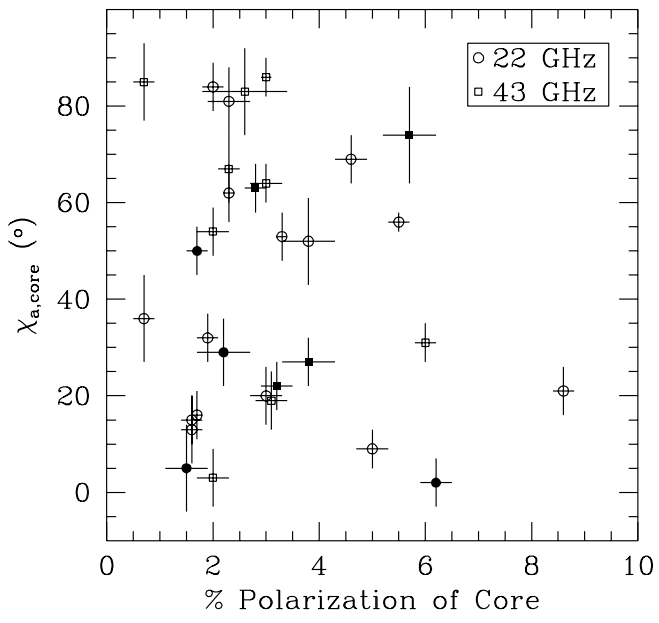

Fig. 2*a*

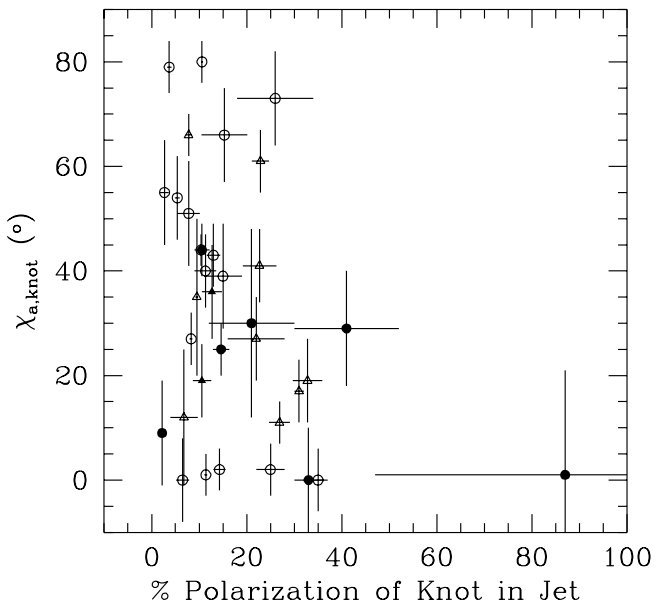

Fig. 2*b*

Fig. 2.—Position angle of polarization electric vector relative to the local jet direction vs. percent polarization for (*a*) cores and (*b*) knots in the jets. *Open symbols*: quasars; *filled symbols*: BL Lac objects. In panel (*b*) moving knots are designated by circles and stationary features by triangles, with no distinction between frequencies.

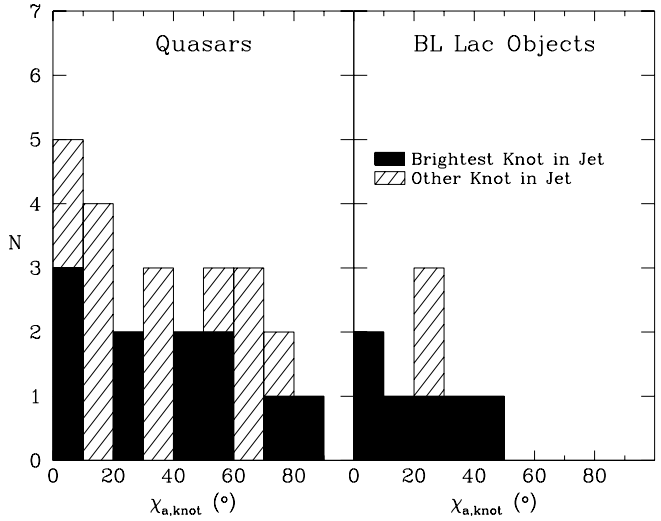

FIG. 3.—Histogram of polarization electric vector directions relative to the local jet direction for features in the jets. The brightest moving features in their respective jets correspond to the filled areas.

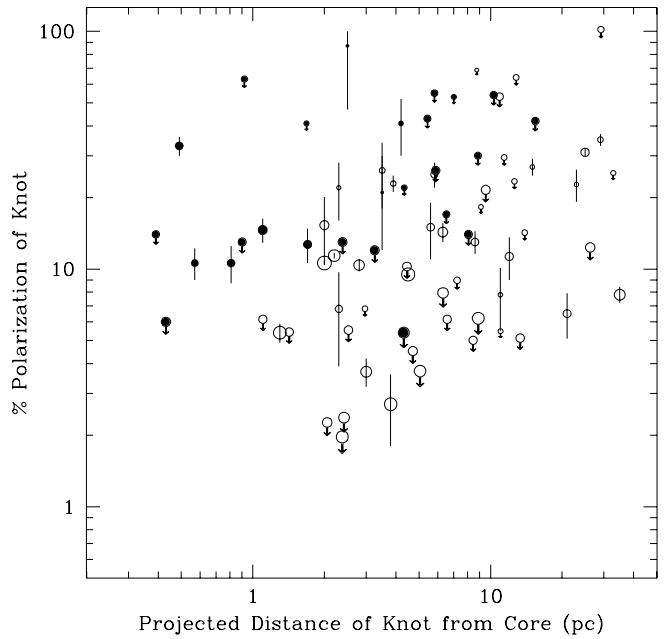

FIG. 5.—Percent polarization vs. projected linear distance from the core for knots in the jets. Upper limits are denoted by arrows. Open symbols represent quasars, and filled symbols correspond to BL Lac objects. The symbols are larger for features with higher flux densities.

0827+243 (semihalo), 0917+449, 1101+384 (Mrk 421), 1622−253, 1652+398 (Mrk 501), 1739+522 (semihalo), 1741−038, and 2209+236. These include the two TeV-bright blazars in our sample (Mrk 421 and Mrk 501). Such polarization patterns may correspond to toroidal magnetic fields, providing some evidence for a magnetically driven jet, as in case 2 above. In addition, there are two other examples of strong polarization observed significantly upstream of the core (designated as "P" components in Table 2): 0336−019 and 0420−014. Such regions signify very well-ordered magnetic fields where the synchrotron emission is faint, perhaps because radiative losses have depleted the population of electrons with energies sufficiently high to radiate at 22 or 43 GHz.

As mentioned in the previous section, the distribution of χ_a of features in the jet implies that the magnetic fields in knots are generally oblique to the jet axis. The absence of a correlation between χ_a (knot) and the ratio of flux density of a knot to that of the core provides no support to models in which the knots are shocks whose fronts are transverse to the jet axis. On the other hand, if many of the jets are directed at angles to the line of sight much less than Γ^{-1}, as expected for a sample selected for extreme relativistic beaming, then the projected magnetic field will not be strongly related to the direction of the jet, since the shock front would be observed nearly face-on.

We conclude that, in comparison with extragalactic radio sources selected solely on the basis of radio properties (e.g., Lister 2001), γ-ray bright blazars possess no observable signature of either jet morphology or polarization structure. The primary correlation is with extreme apparent superluminal motion, as found by Jorstad et al. (2001b). On the other hand, Jorstad et al. (2001a) did find that, just prior to a γ-ray flare, there is a brief reduction in polarization integrated over the entire source. Our single-epoch observations would not be sensitive to such an effect. This points to the need for well–time-sampled polarization-sensitive VLBA observations of γ-ray blazars that will be monitored by future space missions such as the planned *Gamma-Ray Large Area Space Telescope* (*GLAST*).

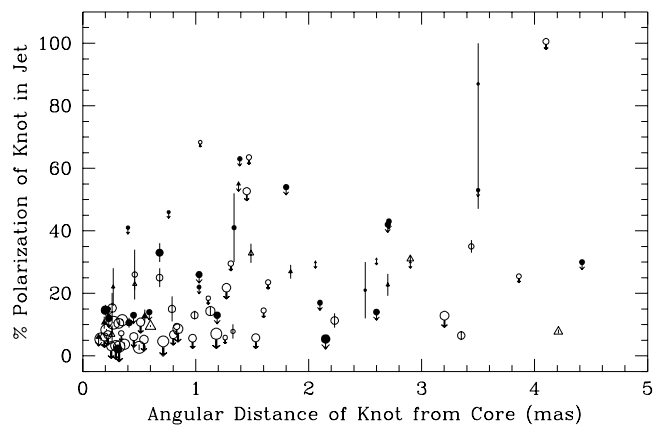

FIG. 4.—Percent polarization vs. angular distance from the core for knots in the jets. Upper limits are denoted by arrows. Circles correspond to moving knots and triangles correspond to stationary features. Open symbols represent quasars, and filled symbols correspond to BL Lac objects. The symbols are larger for features with higher flux densities.

We thank H. Teräsranta for providing flux densities measured at Metsähovi in advance of publication. This work was supported in part by NASA through *CGRO* Guest Investigator grants NAG 5-7323 and NAG 5-2508, and by US National Science Foundation grant AST 98-02941. J. R. M. and A. E. W. were supported in part by the NASA Long Term Space Astrophysics program. The calibration made use of data from the University of Michigan Radio Astronomy Observatory, which is supported by the National Science Foundation and by funds from the University of Michigan. The VLBA is a facility of the National Radio Astronomy Observatory, operated by Associated Universities, Inc., under cooperative agreement with the National Science Foundation.

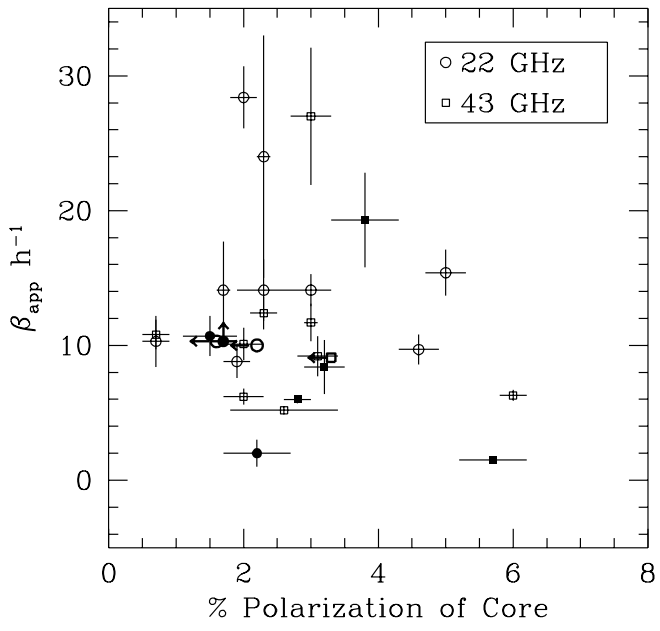

FIG. 6*a*

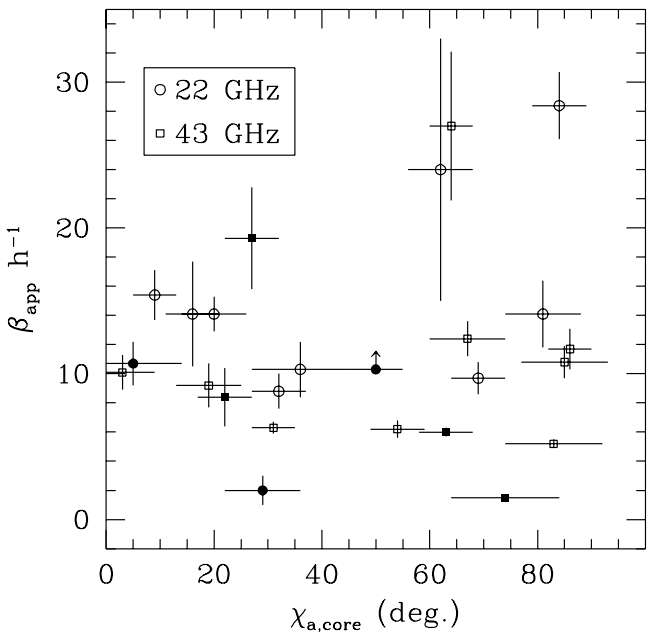

FIG. 6*b*

FIG. 6.—Apparent velocity of moving knots vs. (*a*) percent polarization of the core and (*b*) polarization electric vector direction of the core relative to the direction of the jet immediately downstream of the core. For a given object, only the knot with the fastest well-determined proper motion is included. Open symbols represent quasars, and filled symbols correspond to BL Lac objects. Upper limits to the percent polarization and lower limits to the apparent velocity are indicated by arrows. Seven quasars with no motion reported by Jorstad et al. (2001b) are excluded.

REFERENCES

Akritas, M. G., & Siebert, J. 1996, MNRAS, 278, 919
Buckley, J. H. 1999, Astropart. Phys., 11, 119
Conway, J. E., et al. 1992, ApJ, 396, 62
Gabuzda, D. C., & Cawthorne, T. V. 2000, MNRAS, 319, 1056
Gómez, J. L., Marscher, A. P., Alberdi, A., Jorstad, S. G., & Agudo, I. 2002, VLBA Scientific Memo 30 (NRAO)
Hartman, R. C., et al. 1999, ApJS, 123, 79
Jorstad, S. G., Marscher, A. P., Mattox, J. R., Aller, M. F., Aller, H. D., Wehrle, A. E., & Bloom, S. D. 2001a, ApJ, 556, 738
Jorstad, S. G., Marscher, A. P., Mattox, J. R., Wehrle, A. E., Bloom, S. D., & Yurchenko, A. V. 2001b, ApJS, 134, 181
Laing, R. A. 1980, MNRAS, 193, 439
Leppänen, K. J., Zensus, J. A., & Diamond, P. J. 1995, AJ, 110, 2479
Lister, M. L. 2001, ApJ, 562, 208
Lister, M. L., & Marscher, A.P. 1999, Astropart. Phys., 11, 65
Lister, M. L., Marscher, A. P., & Gear, W. K. 1998, ApJ, 504, 702
Marscher, A.P. 1999, Astropart. Phys., 11, 19
Mattox, J. R., Schacter, J., Molnar, L., Hartman, R. C., & Patnaik, A. R., 1997, ApJ, 481, 95
Meier, D. L., Koide, S., & Uchida, Y. 2001, Science, 291, 84
Pearson, T. J., & Readhead, A. C. S. 1988, ApJ, 328, 114
Shepherd, M. C. 1997, in ASP Conf. Proc. 125, Astronomical Data Analysis Software and Systems VI, ed. G. Hunt & H. E. Payne (San Francisco: ASP), 125
Taylor, G. B. 2000, ApJ, 533, 95
Wardle, J. F. C., & Kronberg, P. P. 1974, ApJ, 194, 249